Suitability of passive RC-network-based inductorless bridged-T as a bandpass NGD circuit

Sébastien Lalléchére, Jamel Nebhen, Yang Liu, George Chan, Glauco Fontgalland, Wenceslas Rahajandraibe, Fayu Wan, Blaise Ravelo

Suitability of passive RC-network based inductorless bridged-T as a bandpass NGD circuit

Sébastien Lallechere
Institut Pascal, Universite Clermont Auvergne, Clermont-Ferrand, France
Jamel Nebhen
Prince Sattam Bin Abdulaziz University, Al Kharj, Saudi Arabia
Yang Liu
Altran, Paris, France
George Chan
ASM Pacific Technology Ltd, Kwai Chung, Hong Kong
Glauco Fontgalland
Federal University of Campina Grande, Campina Grande, Brazil
Wenceslas Rahajandraibe
IM2NP, Aix-Marseille-University, Aix en Provence, France, and
Fayu Wan and Blaise Ravelo
Nanjing University of Information Science and Technology, Nanjing, China

Abstract

Purpose – The passive network topology is used as a bandpass (BP) negative group delay (NGD) function.

Design/methodology/approach – The BP NGD topology under study is composed of an inductorless passive RC network. The circuit analysis is elaborated from the equivalent impedance matrix. Then, the analytical model of the C-shunt bridged-T topology voltage transfer function is established. The BP NGD analysis of the considered topology is developed in function of the bridged-T parameters. The NGD properties and characterizations of the proposed topology are analytically expressed. Moreover, the relevance of the BP NGD theory is verified with the design and fabrication of SMD components-based proof-of-concept (PoC).

Findings – From measurement results, the BP NGD network with −151 ns at the center frequency of 1 MHz over −6.6 dB attenuation is in very good agreement with the C-shunt bridged-T PoC.

Originality/value – This paper develops a mathematical modeling theory and measurement of a C-shunt bridged-T network circuit.

Keywords Bandpass (BP) negative group delay (NGD), Bridged-T topology, Circuit theory, Design method, Inductorless passive network

Paper type Research paper

1. Introduction

The success of the telecommunication technological race depends on the research progress of electronic circuit designs. The analog filters are one of the key elements constituting the transceivers in communication and electronic systems such as those found in television equipment (Adrick, 2013). Constant circuit design improvement of transceivers constituting elements as filters is necessary (Geffe, 1997). Among the existing filter topologies, the bridged-T cells are more and more exploited for designing with various networks (Mohan, 1977; Twin-T Notch Filter Design Tool, 2020). This particular analog circuit topology was also developed to improve the RF and microwave filter performances as the compactness improvement and size reduction (Wang and Lin, 2019; Yao *et al.*, 2009; Lin and Lee, 2013). The bridged-T topology was also extended to design structures as coils, which can be used to miniaturize microwave devices as power dividers (Lin and Lee, 2012). Nonetheless, further circuit theory must be developed to improve the design method of bridged-T-based functions.

This work was supported by the Deanship of Scientific Research at Prince Sattam bin Abdulaziz University, Saudi Arabia. This research work was also supported in part by NSFC under Grant 61971230 and in part by Jiangsu Specially Appointed Professor program and Six Major Talents Summit of Jiangsu Province (2019-DZXX-022) and in part by the Startup Foundation for Introducing Talent of NUIST, in part by the Post-graduate Research and Practice Innovation Program of Jiangsu Province under Grant KYCX20_0966.

Data availability: Data sharing is not applicable to this article as no data sets were generated or analyzed during the current study.

For example, an attempt of low-sensitive filters was designed in (Moschytz, 1999). However, the achievement of low-power consumption is limited by the use of systematically lossy RC-topology. Moreover, the bridged-T topologies were also exploited to design delay circuit correctors. However, the kind of existing bridged-T-based delay correctors operates with additional delays, which are susceptible to limit the communication system performances. In addition, with the popular development of computer-aided design equipment, the electronic design engineers' trend to design bridged-T circuits is only based on simulation tools (Toumazou *et al.*, 2002).

As an alternative to delaying correction, we would like to propose the use of the negative group delay (NGD) circuit (Ravelo *et al.*, 2020a), which enables to cancel out the undesirable delays. However, because of its inherent counterintuitive aspect, the analysis and design method of NGD circuits remains an open question to electronic and communication system design engineers. For this reason, the present paper develops original inductorless topologies of bandpass (BP) NGD circuit theory. Bridged-T circuits implemented with RC-networks constitute the BP NGD topology.

Before the exploration of the original BP NGD theory of inductorless bridged-T circuit, a state of the art on NGD circuit design has to be described. The NGD effect was investigated theoretically and experimentally with electronic circuits in the 1990s (Mitchell and Chiao, 1998; Mitchell and Chiao, 1997). It was emphasized that the NGD signature corresponds to the propagation of electronic smoothed signals with leading and trailing edges in time advance (Mitchell and Chiao, 1998; Mitchell and Chiao, 1997; Nakanishi *et al.*, 2002; Kitano *et al.*, 2003; Munday and Henderson, 2004; Jian-Wu and Zheng-He, 2015; Wan *et al.*, 2019b; Mao *et al.*, 2019). This counterintuitive time advance propagation of NGD signal does not contradict the causality principle (Mitchell and Chiao, 1998; Mitchell and Chiao, 1997). This counterintuitive aspect renders the NGD effect an unfamiliar function to most electronic function-based physicists and engineers. Despite the counterintuitive behavior of the NGD phenomenon, synthesis and design of diverse NGD circuits were proposed past decade (Ahn *et al.*, 2009; Abuelma'atti and Khalifa, 2018; Meng *et al.*, 2018). The synthesis of a second-order distributed NGD circuit was proposed in (Ahn *et al.*, 2009). More recently, an active NGD circuit using an operational amplifier (Abuelma'atti and Khalifa, 2018) and a bi-directional amplifier (Meng *et al.*, 2018) were introduced to compensate for the attenuation losses. However, electronic circuit design engineers remain skeptical, unfamiliar and do not want to explore the NGD function because of a lack of pedagogical understanding.

Against this misunderstanding, more obvious academic research was initiated on the familiarity to the NGD function by establishing an analogy with the filter behavior (Ravelo, 2014; Ravelo, 2017). The concept of low-pass, high-pass and band-pass (BP) NGD function related to the sign of the group delay (GD) in the operation frequency band was introduced (Ravelo, 2014; Ravelo, 2017). Despite this seemingly obvious pedagogy, further research work has to be conducted on the different properties and characteristics of the NGD circuit topology. Transitively, the present paper provides a mathematical modeling theory and measurement of a new BP NGD topology of the capacitor-shunt-based bridged-T passive cell without using the inductance component never been studied before. The main differences of the proposed research work with the existing ones (Ravelo *et al.*, 2020a; Mitchell and Chiao, 1998; Mitchell and Chiao, 1997; Nakanishi *et al.*, 2002; Kitano *et al.*, 2003; Munday and Henderson, 2004; Jian-Wu and Zheng-He, 2015; Wan *et al.*, 2019b; Mao *et al.*, 2019; Ahn *et al.*, 2009; Abuelma'atti and Khalifa, 2018; Meng *et al.*, 2018; Ravelo, 2014; Ravelo, 2017; Myoung *et al.*, 2007; Vemagiri *et al.*, 2007; Wan *et al.*, 2019a; Ravelo, 2013; Ravelo *et al.*, 2020b; Ravelo *et al.*, 2021) are:

- A BP NGD theory of inductorless passive circuit based on a C-shunt-based bridged-T network is developed. The developed circuit theory is focused on the impedance matrix approach and also the GD expression elaboration of the new BP NGD topology implemented with an inductorless passive lumped circuit.
- The voltage transfer function (VTF)-based BP NGD canonical form of the considered inductorless passive topology is elaborated.
- The NGD analysis not familiar to the electronic design engineers including the calculation of NGD center frequency, NGD cut-off frequencies, NGD value and attenuation at specific frequencies is developed from the VTF.

By the way, this paper is organized into five sections as follows:

- Section 2 introduces the basic characteristics of the BP NGD function. The main specific parameters to qualify an NGD function will be defined. More importantly, an analytical expression of the VTF will be explored. After the analysis in the branch and mesh spaces, the impedance matrix general expression will be established. Then, the VTF of the bridged-T general topology will be expressed.
- Section 3 presents the NGD theory of an inductorless bridged-T topology built with a shunt capacitor network. The BP NGD properties and characteristics of the bridged-T will be developed.
- Section 4 focuses on practical validation. Doing this, the comparison between analytical model, simulation and measurement results will be discussed by designing an SMD component-based circuit prototype as a proof-of-concept (PoC).
- Section 5 opens a discussion on some potential applications of BP NGD circuits.
- Section 6 concludes the paper.

2. Theory of bandpass negative group delay function

This section describes the unfamiliar BP NGD function theory. The basic definition of BP NGD function will be introduced. The principal specifications are presented. The BP NGD canonical form will be analyzed in function of specific parameters.

2.1 Key parameters for the negative group delay analysis

The general topology of the bridged-T circuit under study can be assumed as a two-port system as depicted by Figure 1(a). The circuit configuration of the impedance element-based

Figure 1 NGD circuit

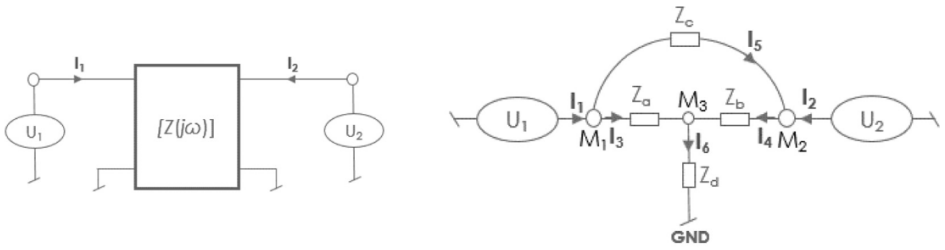

(a) (b)

Notes: (a) Two-port system black box; (b) general topology of the bridged-T network under study

topology is represented in Figure 1(b). This passive circuit is composed of elementary four components represented by impedances, Z_κ with a subscript, $\kappa = a, b, c, d$.

According to the circuit theory, by denoting the angular frequency variable, ω, the two-port system can be modeled with the impedance matrix:

$$[Z(s)] = \begin{bmatrix} Z_{11}(s) & Z_{12}(s) \\ Z_{21}(s) & Z_{22}(s) \end{bmatrix} \tag{1}$$

This matrix is combined to the vectors of access voltage:

$$[U(s)] = \begin{bmatrix} U_1(s) \\ U_2(s) \end{bmatrix} \tag{2}$$

and current:

$$[I(s)] = \begin{bmatrix} I_1(s) \\ I_2(s) \end{bmatrix} \tag{3}$$

by the matrix relation:

$$\begin{bmatrix} U_1(s) \\ U_2(s) \end{bmatrix} = [Z(s)] \times \begin{bmatrix} I_1(s) \\ I_2(s) \end{bmatrix} \tag{4}$$

The associated VTF is defined by the equation:

$$T(s) = \frac{U_2(s)}{U_1(s)}|_{I_2(s)=0} = \frac{Z_{21}(s)}{Z_{11}(s)}. \tag{5}$$

The Kirchhoff voltage law applied to nodes M_1 and M_2, gives, respectively:

$$\begin{cases} U_1(s) = V_{M_3}(s) + Z_a(s)I_3(s) \\ U_2(s) = V_{M_3}(s) + Z_b(s)I_4(s) \end{cases}. \tag{6}$$

The application of Millman's theorem at the node M_3 implies:

$$V_{M_3}(s) = \frac{\frac{U_1(s)}{Z_a(s)} + \frac{U_2(s)}{Z_b(s)}}{\frac{1}{Z_a(s)} + \frac{1}{Z_b(s)} + \frac{1}{Z_d(s)}}. \tag{7}$$

Currents I_3 and I_4 can be written as:

$$\begin{cases} I_3(s) = I_1(s) - \dfrac{U_1(s) - U_2(s)}{Z_c(s)} \\ I_4(s) = I_2(s) + \dfrac{U_1(s) - U_2(s)}{Z_c(s)} \end{cases}. \tag{8}$$

Then, substituting equations (7) and (8) into the equation (6), we can derive:

$$\begin{cases} U_1(s) = \dfrac{Z_d(s)\begin{bmatrix} Z_b(s)U_1(s) + \\ Z_a(s)U_2(s) \end{bmatrix}}{Z_a(s)Z_b(s) + Z_d(s)[Z_a(s) + Z_b(s)]} + Z_a(s)I_3(s) \\ U_2(s) = \dfrac{Z_d(s)\begin{bmatrix} Z_b(s)U_1(s) + \\ Z_a(s)U_2(s) \end{bmatrix}}{Z_a(s)Z_b(s) + Z_d(s)[Z_a(s) + Z_b(s)]} + Z_b(s)I_4(s) \end{cases}. \tag{9}$$

It yields from these two last equations the impedance matrix elements expressed as:

$$\begin{cases} Z_{11}(s) = \dfrac{Z_a(s)[Z_b(s) + Z_c(s) + Z_d(s)] + Z_d(s)[Z_c(s) + Z_d(s)]}{Z_{den}(s)} \\ Z_{12}(s) = Z_{21}(s) = \dfrac{[Z_a(s) + Z_d(s)][Z_c(s) + Z_d(s)]}{Z_{den}(s)} \\ Z_{22}(s) = \dfrac{[Z_a(s) + Z_d(s)][Z_b(s) + Z_c(s)] + Z_b(s)Z_c(s)}{Z_{den}(s)} \end{cases}. \tag{10}$$

with:

$$Z_{den}(s) = Z_a(s) + Z_b(s) + Z_c(s). \tag{11}$$

Therefore, the VTF given in equation (3) becomes:

$$T(s) = \frac{Z_a(s)[Z_b(s) + Z_d(s)] + Z_d(s)[Z_b(s) + Z_c(s)]}{Z_a(s)[Z_b(s) + Z_c(s) + Z_d(s)] + Z_d(s)[Z_b(s) + Z_c(s)]}. \tag{12}$$

To analyze the system, we can use the magnitude and phase of this VTF expressed as, respectively:

$$T(\omega) = |T(j\omega)| = \sqrt{\mathrm{Re}[T(j\omega)]^2 + \mathrm{Im}[T(j\omega)]^2}. \tag{13}$$

$$\varphi(\omega) = \arg\{\mathrm{Im}[T(j\omega)]/\mathrm{Re}[T(j\omega)]\}. \quad (14)$$

By definition, the analytical expression of the GD is given by:

$$GD(\omega) = -\partial\varphi(\omega)/\partial\omega. \quad (15)$$

The BP NGD analysis is elaborated from these fundamental analytical definitions.

2.2 Bandpass negative group delay analysis

The following steps described the main methodological actions for the achievement of the BP NGD analysis. It is noteworthy that the present theory is built under the hypothesis of a system represented by passive circuits.

2.2.1 Step 1: Group delay calculation

The NGD circuit analysis of an unknown circuit must begin with the previously introduced expression of GD, which can be obtained via the calculation of the impedance matrix $[Z(j\omega)]$. Once the GD expression in equation (8) is defined, the BP NGD analysis can be started with the following steps.

2.2.2 Step 2: Negative group delay existence condition

The key mathematical analysis for starting the NGD analysis consists in proving the existence of NGD which can be analytically formulated by the in equation with an unknown interval of ω:

$$GD(\omega) < 0. \quad (16)$$

If the previous equation does not have a solution, it means that we are facing a completely positive group delay system. In this case, the conclusion can be made and it is not necessary to continue the next steps.

2.2.3 Step 3: Negative group delay optimal value

This step consists of the identification of NGD center angular frequencies ω_o where the NGD can reach its minimal negative value. If the GD can be negative over a frequency band, it is necessary to identify the NGD center angular frequency, ω_o where the NGD can reach its minimal negative value:

$$GD_{\min} = GD(\omega_o) < 0. \quad (17)$$

For the case of ω_o = 0, the system is classified as a low-pass NGD function (Ravelo, 2014; Ravelo, 2017). The mathematical equation is not always mathematically easy to solve especially for the case of an electrical system constituted by distributed and non-linear topologies. Even if we place under the case of linear circuit constituted only by lumped R, L and C elements, the expressions of GD are usually constituted by polynomial equations with at least a second-order degree. To avoid the mathematical roadblocks, the NGD engineer can proceed with any numerical solvers and also proceed by intuition for the case of complex topologies.

2.2.4 Step 4: Negative group delay bandwidth

Figure 2(a) represents the GD ideal response of BP NGD function with the specific NGD value, $-\tau_0$. The NGD center frequency is denoted ω_o.

The NGD cut-off frequencies, denoted, $\omega_{a,b}$, are the roots of the equation:

Figure 2 Ideal typical (a) GD and (b) magnitude responses of BP NGD function

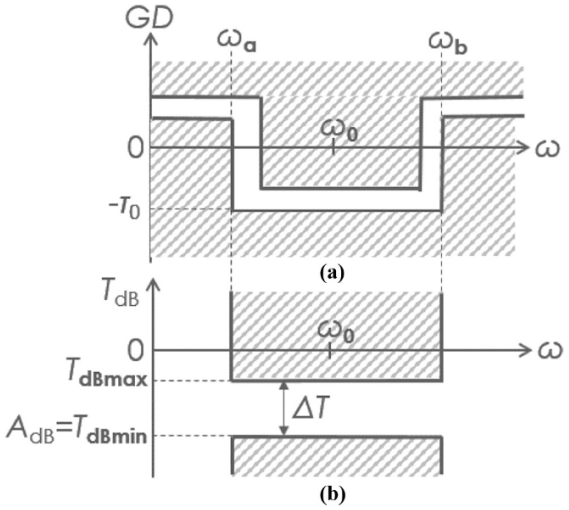

$$GD(\omega) = 0. \quad (18)$$

By assuming that, $\omega_a < \omega_b$, the NGD bandwidth can be determined by the relation:

$$\Delta\omega_{NGD} = \omega_b - \omega_a. \quad (19)$$

The GD is ideally specified by:

$$\begin{cases} GD(\omega < \omega_a) > 0 \\ GD(\omega_a < \omega < \omega_b) < 0 \\ GD(\omega_b < \omega) > 0 \end{cases}. \quad (20)$$

In addition to the GD, the magnitudes of reflection and transmission coefficients must be assessed.

2.2.5 Step 5: Transmittance attenuation specifications

Similar to classical electronic functions, the NGD circuit must operate under specifications related to the attenuation limitation. Substantially, we can represent the constraint related to the attenuation in the NGD bandwidth in Figure 2(b). For example, we can denote the attenuation limit, A, according to the expected application of the NGD function. Subsequently, the NGD loss can be formulated with the following condition:

$$T(\omega) > |T(j\omega)|_{\min} = A. \quad (21)$$

It is interesting to note that for the linear circuits, we have the optimal angular frequency related to the magnitude:

$$\begin{cases} -\tau_o = GD(\omega_o) < 0 \\ |T(j\omega)|_{\min} = |T(j\omega_o)| \end{cases}. \quad (22)$$

Thus, the optimal angular frequency ($\omega_{opt} \neq \omega_o$) related to the GD is defined by:

$$\begin{cases} GD_{\min} = GD(\omega_{opt}) < 0 \\ |T(j\omega_o)| \neq 0 \end{cases}. \tag{23}$$

The feasibility of this BP NGD theory will be concretized with inductorless bridged-T topology investigated in the next sections.

3. Bandpass negative group delay investigation of inductorless bridged-T topology with shunt capacitor

The present section develops the BP NGD analysis of inductorless bridged-T topology with a shunt capacitor. The theoretical concept will be validated with simulations. The BP NGD analysis will be presented after the topological description and the VTF canonical identification.

3.1 Topological description

The proposed inductorless bridged-T topology is built with elementary impedances defined analytically by:

$$Z_a(s) = R_a = R \tag{24}$$

$$Z_b(s) = R_b = xR \tag{25}$$

$$Z_c(s) = 1/(sC_c) = 1/(sC) \tag{26}$$

$$Z_d(s) = 1/(sC_d) = 1/(syC). \tag{27}$$

The corresponding inductorless bridged-T network is depicted in Figure 3.

To confirm if the shunt capacitor bridged-T cell of Figure 3 behaves as a BP NGD function, its VTF should present the canonical form. The present study aims to the development of the most fundamental expression of BP NGD TF. The canonical form is defined with the basic specifications indicated in Figure 2. The simplest BP NGD TF should be a second-order system. Substantially, the canonical form of BP NGD TF can be expressed by the second-order polynomial formula:

Figure 3 Shunt capacitor-based bridged-T cell

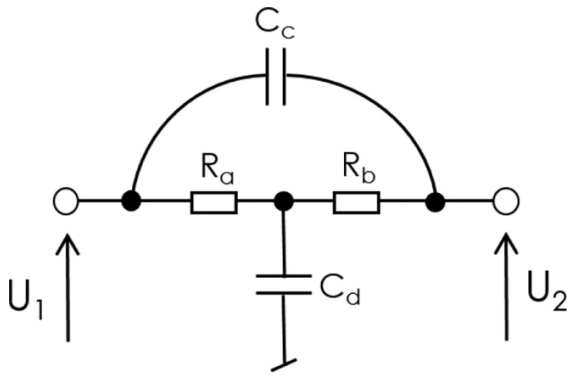

$$T(s) = K\left(\frac{s^2 + \omega_\eta s + \omega_0^2}{s^2 + \omega_\psi s + \omega_0^2}\right) \tag{28}$$

with the characteristic parameters, K as a positive real, ω_0 depicts the NGD center frequency and parameters ω_η and ω_ψ. The corresponding transmittance is obtained substituting $s = j\omega$, and therefore, we have:

$$T(j\omega) = K\left(\frac{\omega_0^2 - \omega^2 + j\omega_\eta\omega}{\omega_0^2 - \omega^2 + j\omega_\psi\omega}\right) \tag{29}$$

By means of equations (13) and (14), the associated magnitude and phase can be expressed as, respectively:

$$T(\omega) = K\frac{\sqrt{\left(\omega_0^2 - \omega^2\right)^2 + (\omega_\eta\omega)^2}}{\sqrt{\left(\omega_0^2 - \omega^2\right)^2 + (\omega_\psi\omega)^2}} \tag{30}$$

$$\varphi(\omega) = \arctan\left(\frac{\omega_\eta\omega}{\omega_0^2 - \omega^2}\right) - \arctan\left(\frac{\omega_\psi\omega}{\omega_0^2 - \omega^2}\right) \tag{31}$$

The GD can be derived from the previous equation by means of equation (15).

3.2 Identification of bandpass negative group delay canonical form

For the BP NGD, the corresponding VTF can be identified with the canonical form introduced in equation (28) by taking the parameters $T_0 = 1$ and:

$$\omega_0 = \varpi/\sqrt{xy} \tag{32}$$

$$\omega_\eta = (1+x)\varpi/(xy) \tag{33}$$

$$\omega_\psi = (1+x+y)\varpi/(xy) \tag{34}$$

with:

$$\varpi = 1/(RC). \tag{35}$$

The optimal VTF magnitude at the center frequency is:

$$T(\omega_0) = (x+1)/(x+y+1). \tag{36}$$

The GD given by equation (22) becomes:

$$GD(\omega_0) = \frac{-2xy^2RC}{(1+x)(1+x+y)}. \tag{37}$$

It is important to underline that this GD is always negative. It means that the necessary condition for the BP NGD existence is verified. The associated NGD cut-off frequencies which are the roots of GD-based equation (18) are formulated as:

$$\omega_a = \frac{\varpi\sqrt{1+y+x(2+x+3y) - \sqrt{\zeta_c}}}{xy\sqrt{2}} \tag{38}$$

$$\begin{cases} GD_{\min} = GD(\omega_{opt}) < 0 \\ |T(j\omega_o)| \neq 0 \end{cases}. \tag{23}$$

The feasibility of this BP NGD theory will be concretized with inductorless bridged-T topology investigated in the next sections.

3. Bandpass negative group delay investigation of inductorless bridged-T topology with shunt capacitor

The present section develops the BP NGD analysis of inductorless bridged-T topology with a shunt capacitor. The theoretical concept will be validated with simulations. The BP NGD analysis will be presented after the topological description and the VTF canonical identification.

3.1 Topological description

The proposed inductorless bridged-T topology is built with elementary impedances defined analytically by:

$$Z_a(s) = R_a = R \tag{24}$$

$$Z_b(s) = R_b = xR \tag{25}$$

$$Z_c(s) = 1/(sC_c) = 1/(sC) \tag{26}$$

$$Z_d(s) = 1/(sC_d) = 1/(syC). \tag{27}$$

The corresponding inductorless bridged-T network is depicted in Figure 3.

To confirm if the shunt capacitor bridged-T cell of Figure 3 behaves as a BP NGD function, its VTF should present the canonical form. The present study aims to the development of the most fundamental expression of BP NGD TF. The canonical form is defined with the basic specifications indicated in Figure 2. The simplest BP NGD TF should be a second-order system. Substantially, the canonical form of BP NGD TF can be expressed by the second-order polynomial formula:

Figure 3 Shunt capacitor-based bridged-T cell

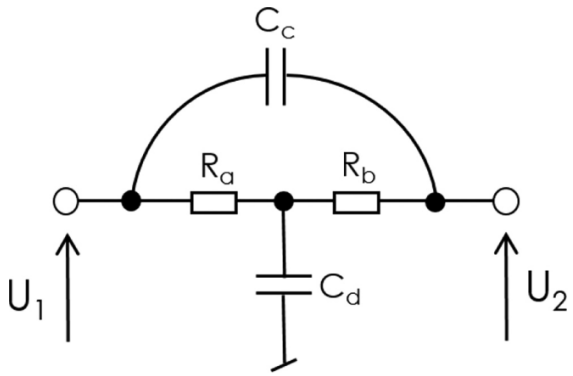

$$T(s) = K\left(\frac{s^2 + \omega_\eta s + \omega_0^2}{s^2 + \omega_\psi s + \omega_0^2}\right) \tag{28}$$

with the characteristic parameters, K as a positive real, ω_0 depicts the NGD center frequency and parameters ω_η and ω_ψ. The corresponding transmittance is obtained substituting $s = j\omega$, and therefore, we have:

$$T(j\omega) = K\left(\frac{\omega_0^2 - \omega^2 + j\omega_\eta\omega}{\omega_0^2 - \omega^2 + j\omega_\psi\omega}\right) \tag{29}$$

By means of equations (13) and (14), the associated magnitude and phase can be expressed as, respectively:

$$T(\omega) = K\frac{\sqrt{\left(\omega_0^2 - \omega^2\right)^2 + (\omega_\eta\omega)^2}}{\sqrt{\left(\omega_0^2 - \omega^2\right)^2 + (\omega_\psi\omega)^2}} \tag{30}$$

$$\varphi(\omega) = \arctan\left(\frac{\omega_\eta\omega}{\omega_0^2 - \omega^2}\right) - \arctan\left(\frac{\omega_\psi\omega}{\omega_0^2 - \omega^2}\right) \tag{31}$$

The GD can be derived from the previous equation by means of equation (15).

3.2 Identification of bandpass negative group delay canonical form

For the BP NGD, the corresponding VTF can be identified with the canonical form introduced in equation (28) by taking the parameters $T_0 = 1$ and:

$$\omega_0 = \varpi/\sqrt{xy} \tag{32}$$

$$\omega_\eta = (1+x)\varpi/(xy) \tag{33}$$

$$\omega_\psi = (1+x+y)\varpi/(xy) \tag{34}$$

with:

$$\varpi = 1/(RC). \tag{35}$$

The optimal VTF magnitude at the center frequency is:

$$T(\omega_0) = (x+1)/(x+y+1). \tag{36}$$

The GD given by equation (22) becomes:

$$GD(\omega_0) = \frac{-2xy^2RC}{(1+x)(1+x+y)}. \tag{37}$$

It is important to underline that this GD is always negative. It means that the necessary condition for the BP NGD existence is verified. The associated NGD cut-off frequencies which are the roots of GD-based equation (18) are formulated as:

$$\omega_a = \frac{\varpi\sqrt{1+y+x(2+x+3y) - \sqrt{\zeta_c}}}{xy\sqrt{2}} \tag{38}$$

Figure 5 (a) Plot of $(\omega_0\tau_0)_{max}$ and τ_{0max} (b) versus attenuation A

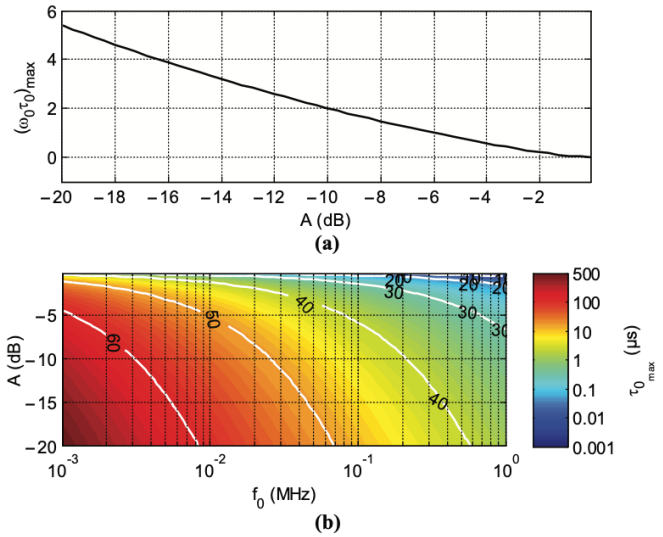

Figures 6(a) and 6(b) present the mapping plots of the coefficients, x and y, versus the attenuation and the center frequency-GD product. The coefficients, x and y, vary between $x_{min} = 10^{-5}$ and $x_{max} = 444$ and $y_{min} = 0.12$ and $y_{max} = 332$, with maximum value not shown in the plot.

To verify the feasibility of the developed BP NGD theory, a practical investigation with a PoC circuit will be presented in the next section.

4. Application and validation results

This section is focused on the application study. To do this, sensitivity analyses of the C-shunt bridged-T PoC circuit will be explored. The present BP NGD validation study is performed by comparisons of calculated, simulated and measured PoC prototypes. The calculated, simulation and experimentation results will be discussed in the following paragraphs.

4.1 Synthesis calculation results of bridged-T circuit parameters from bandpass negative group delay specifications

First of all, the BP NGD behavioral aspect of our bridged-T passive circuit under study was analyzed following the methodology described by Subsection 2.2. Afterwards, the synthesis of our shunt capacitor-based topology was performed with given arbitrary parameters:

- The NGD center frequency, $f_0 = 1$ MHz.
- The NGD value, $\tau_0 = -150$ ns.
- And the attenuation $A = -6$ dB.

The components were chosen to enable to design and to fabricate a validation PoC circuit of the bridged-T topology constituted by R and C elements available in our laboratories. Accordingly, we have considered by equations (43) and (44) which are established in the theoretical investigation of the previous section.

Figure 6 Mapping plots of (a) x and (b) y versus (A, $\omega_0\tau_0$)

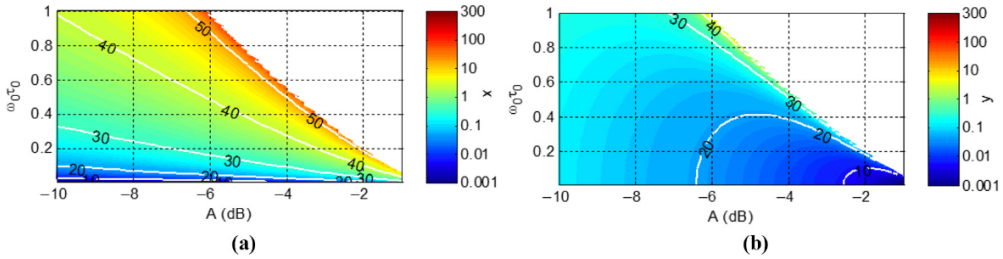

Hence, we calculated the resistor and capacitor elements constituting our bridged-T circuit PoC. The fabricated circuit prototype was implemented with SMD components with nominal values and references indicated in Table 1. To validate definitively the BP NGD aspect, Figure 7(a) shows the schematic of the designed and simulated bridged-T circuit. Hence, the photograph of the prototype is presented in Figure 7(b). The access ports are made of SMA connectors whose effects can be assumed as negligible to the NGD responses.

The PoC circuit was designed on a Cu-metalized FR4 dielectric substrate having physical characteristics addressed in Table 2.

4.2 Sensitivity analyses of C-shunt bridged-T proof-of-concept

The proposed sensitivity analyses (SAs) were performed concerning the resistor, R and capacitor, C. The MATLAB® calculations of magnitude and GD from 0.1 MHz to 5 MHz were carried out based on equations (28) and (15) using impedances expressed in equation (24). The values of resistor and capacitor of the C-shunt bridged-T circuit PoC are addressed in Table 3.

4.2.1 Sensitivity analyses versus R_a

The present sensitivity analysis was performed under the linear variation of resistance component, $R_a = R$. As indicated by Table 3, the minimal and maximal range of the variation is defined between 9.5 Ω to 10.5 Ω. Figures 8(a) and 8(b) display the cartographies of VTF GD and magnitude concerning pair variables (f, R). We can remark the BP NGD behavior with NGD center frequency, f_0 = 1 MHz, which is insensitive to R. The effect of the resistor sensitivity is negligible on the BP NGD performance.

Table 1 References of the SMD components constituting the bridged-T tested circuit.

Nature	Name	Nominal value	Package	Reference	Tolerance (%)
Resistor	R_a	330 Ω	0805	YAGEO	5
	R_b	10 Ω	0805	YAGEO	5
Capacitor	C_c	16 pF	0805	Murata	5
	C_d	8 pF	0805	Murata	5

Table 2 Substrate physical parameters

Structure	Description	Parameters	Values
Substrate	Relative permittivity	ε_r	4.5
	Loss tangent	$\tan(\delta)$	0.02
	Thickness	h	1.6 mm
Metallization conductor	Copper conductivity	σ	58 MS/m
	Thickness	t	35 μm

Table 3 Minimal and maximal values of resistors and capacitors during the SAs

Component	Minimum	Maximum
R_a	9.5 Ω	10.5 Ω
R_b	17.1 Ω	18.9 Ω
C_c	6.46 nF	7.14 nF
C_d	20.9 nF	23.1 nF

4.2.2 Sensitivity analyses versus R_b

Figures 9(a) and 9(b) depict the cartographies of the magnitude and GD of the bridged-T circuit when varying linearly resistance, R_b, following the range indicated in Table 3. We can underline that we have a similar influence as the previous case of study. Resistance, R_b, does not influence the NGD value. However, the NGD bandwidth is slightly decreasing when this resistance value increases.

4.2.3 Sensitivity analyses versus C_c

The present sensitivity analysis was performed concerning the variation of the capacitor $C_a = C$ from 35.02 nF and 38.71 nF by fixing the other component values as addressed in Table 3. Figures 10(a) and 10(b) display the cartographies of computed VTF GD and magnitude in the function of the pair of variables (f, C). A similar interpretation can be deduced from these results, the fluctuation of C is not sensitive to the BP NGD performance.

4.2.4 Sensitivity analyses versus c_d

Figures 11(a) and 11(b) are introducing the cartographies of GD and the magnitude of the bridged-T circuit versus the pair of variables (f, C_b). Once again, we can underline the BP NGD behavior from the GD mapping of Figure 11(a). The SA was performed by linearly varying the capacitor according to the

Figure 7 (a) Schematic and (b) photo of the C-shunt inductorless bridged-T NGD circuit

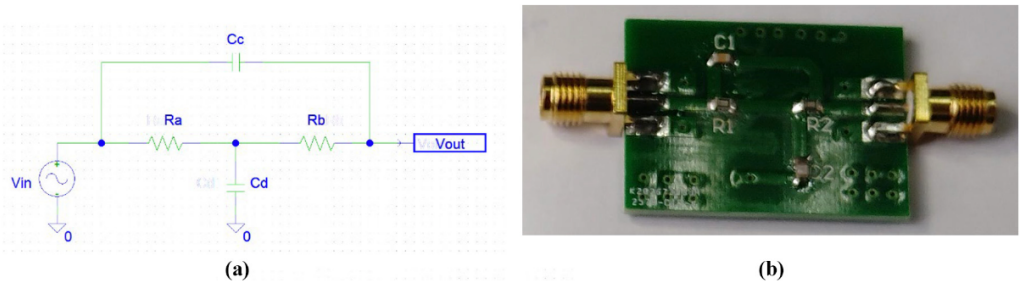

(a) (b)

Hence, we calculated the resistor and capacitor elements constituting our bridged-T circuit PoC. The fabricated circuit prototype was implemented with SMD components with nominal values and references indicated in Table 1. To validate definitively the BP NGD aspect, Figure 7(a) shows the schematic of the designed and simulated bridged-T circuit. Hence, the photograph of the prototype is presented in Figure 7(b). The access ports are made of SMA connectors whose effects can be assumed as negligible to the NGD responses.

The PoC circuit was designed on a Cu-metalized FR4 dielectric substrate having physical characteristics addressed in Table 2.

4.2 Sensitivity analyses of C-shunt bridged-T proof-of-concept

The proposed sensitivity analyses (SAs) were performed concerning the resistor, R and capacitor, C. The MATLAB® calculations of magnitude and GD from 0.1 MHz to 5 MHz were carried out based on equations (28) and (15) using impedances expressed in equation (24). The values of resistor and capacitor of the C-shunt bridged-T circuit PoC are addressed in Table 3.

4.2.1 Sensitivity analyses versus R_a

The present sensitivity analysis was performed under the linear variation of resistance component, $R_a = R$. As indicated by Table 3, the minimal and maximal range of the variation is defined between 9.5 Ω to 10.5 Ω. Figures 8(a) and 8(b) display the cartographies of VTF GD and magnitude concerning pair variables (f, R). We can remark the BP NGD behavior with NGD center frequency, f_0 = 1 MHz, which is insensitive to R. The effect of the resistor sensitivity is negligible on the BP NGD performance.

Table 1 References of the SMD components constituting the bridged-T tested circuit.

Nature	Name	Nominal value	Package	Reference	Tolerance (%)
Resistor	R_a	330 Ω	0805	YAGEO	5
	R_b	10 Ω	0805	YAGEO	5
Capacitor	C_c	16 pF	0805	Murata	5
	C_d	8 pF	0805	Murata	5

Table 2 Substrate physical parameters

Structure	Description	Parameters	Values
Substrate	Relative permittivity	ε_r	4.5
	Loss tangent	$\tan(\delta)$	0.02
	Thickness	h	1.6 mm
Metallization conductor	Copper conductivity	σ	58 MS/m
	Thickness	t	35 μm

Table 3 Minimal and maximal values of resistors and capacitors during the SAs

Component	Minimum	Maximum
R_a	9.5 Ω	10.5 Ω
R_b	17.1 Ω	18.9 Ω
C_c	6.46 nF	7.14 nF
C_d	20.9 nF	23.1 nF

4.2.2 Sensitivity analyses versus R_b

Figures 9(a) and 9(b) depict the cartographies of the magnitude and GD of the bridged-T circuit when varying linearly resistance, R_b, following the range indicated in Table 3. We can underline that we have a similar influence as the previous case of study. Resistance, R_b, does not influence the NGD value. However, the NGD bandwidth is slightly decreasing when this resistance value increases.

4.2.3 Sensitivity analyses versus C_c

The present sensitivity analysis was performed concerning the variation of the capacitor $C_a = C$ from 35.02 nF and 38.71 nF by fixing the other component values as addressed in Table 3. Figures 10(a) and 10(b) display the cartographies of computed VTF GD and magnitude in the function of the pair of variables (f, C). A similar interpretation can be deduced from these results, the fluctuation of C is not sensitive to the BP NGD performance.

4.2.4 Sensitivity analyses versus c_d

Figures 11(a) and 11(b) are introducing the cartographies of GD and the magnitude of the bridged-T circuit versus the pair of variables (f, C_b). Once again, we can underline the BP NGD behavior from the GD mapping of Figure 11(a). The SA was performed by linearly varying the capacitor according to the

Figure 7 (a) Schematic and (b) photo of the C-shunt inductorless bridged-T NGD circuit

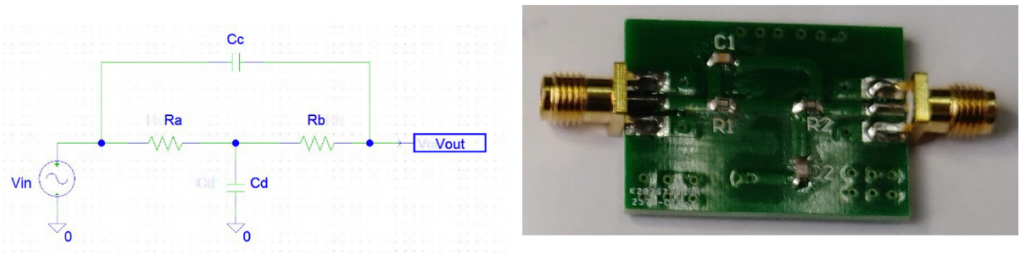

(a) (b)

subsection is divided in three paragraphs. First, the measurement technique of the GD and magnitude responses are explained. Thus, the practical investigation is discussed. Then, a comparative study of the BP NGD performance of the C-shunt inductorless bridged-T topology compared to the existing BP-NGD ones is presented.

4.3.1 Extraction of experimented voltage transfer function magnitude, phase and group delay responses of the tested bridged-T passive circuit prototype

We emphasize that the proposed validation study is carried out by comparisons of calculation from MATLAB®, simulation from ADS® electronic circuit commercial tool and measurements. However, the measurement technique is particularly challenging. Therefore, further explanation of the performed technique is introduced in this paragraph. Indeed, the VTF magnitude and phase measurements were carried out based on the exploitation of the s2p-format touchstone data from the two-dimension S-parameters of the tested circuit prototype. The transform equation of S-parameter data to VTF is elaborated in Ravelo *et al.* (2021). The validation is based on the frequency domain analysis performed from minimal frequency f_{min} = 0.1 MHz to maximal frequency f_{max} = 7 MHz with step f_{step} = 50 kHz frequency step. After the S-parameter measurement, the experimental VTF magnitude and phase of the tested C-shunt bridged-T circuit were generated under the same manner as in Ravelo *et al.* (2021). It is noteworthy that the measured GD was extracted via the discrete equivalent expression of equation (15).

4.3.2 Voltage transfer function magnitude responses

The simulated (labeled "Simu."), calculated (labeled "Calc.") and measured (labeled "Meas.") VTF magnitude responses of the tested bridged-T circuit are introduced in Figure 12. We can see that the simulated, calculated and experimented results are plotted in blue-sky circle-dotted curve, red solid curve and navy-blue dashed curve, respectively. The large frequency band plots of the results from f_{min} to f_{max} are displayed in Figure 12 (a). To show more obviously the BP NGD behavior, the zoomed-in plots of the results are presented in Figure 12(b). We can see clearly a good correlation between the magnitude responses despite the slight differences of the measured results.

The notable differences are mainly due to the component inaccuracies and the measurement systematic errors. In addition, the comparisons of the VTF magnitude's remarkable attenuations at the BP NGD specific frequencies are given in Table 4.

The comparative table addresses the VTF magnitude indicating the attenuations at the particular frequencies of our BP NGD circuit as the NGD center frequency, f_o, the NGD optimal frequency, f_{opt} and the lower and upper NGD cut-off frequencies, f_a and f_b, respectively. It is important to underline here that the attenuation at the considered NGD center frequency is more significant.

4.3.3 Bandpass negative group delay validation responses

The most important validation results representing the GD responses of the bridged-T circuit PoC are plotted in Figure 13. Similar to the magnitude investigation of the previous paragraph, the large frequency band plots of the results from f_{min} to f_{max} are displayed in Figure 13(a). Hence, to represent

Figure 12 Comparisons of simulated, calculated and measured VTF magnitudes displayed in (a) large- and (b) narrow-band plots

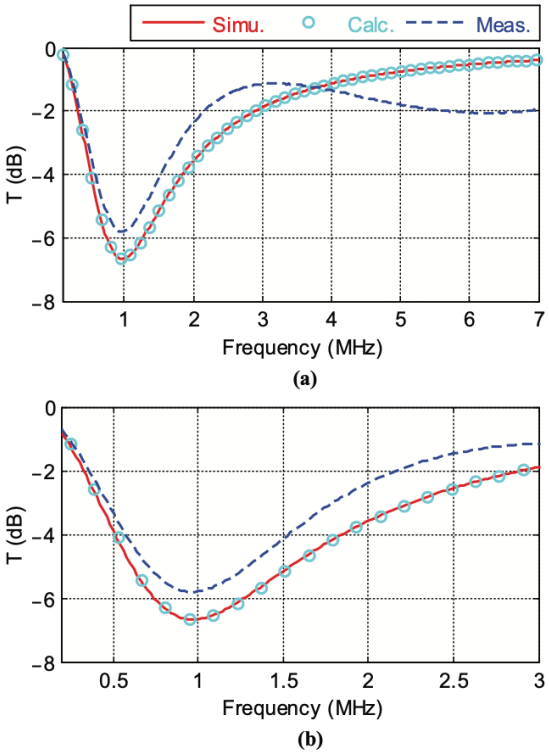

more obviously the BP NGD behavior induced by our bridged-T circuit, the zoomed-in plots of the results are presented in Figure 13(b). Emphatically, these comparative results show a very good agreement between calculation, simulation and measurement despite the slight shift of the GD responses due to the measurement test imperfection. It can be emphasized that the C-shunt bridged-T circuit under study is confirmed to operate with BP NGD behavior. By focusing on the experimental results, we can emphasize that the measured GD is positive in the frequency band when the frequency f is lower than 0.46 MHz and greater than 1.73 MHz. The NGD optimal value τ_{min} = −138.70 ns is achieved at about f_{opt} = 0.88 MHz. Table 5 summarizes the NGD specifications of the tested BP NGD bridged-T circuit from simulation, calculation and measurement.

4.3.4 Comparative study with existing bandpass negative group delay circuits

A comparison of BP NGD specifications between the existing and present work is addressed in Table 6. Different active and passive lumped R, L and C component circuits available in the literature (Mao *et al.*, 2019; Ahn *et al.*, 2009; Abuelma'atti and Khalifa, 2018; Meng *et al.*, 2018; Ravelo, 2014; Wan *et al.*, 2019a; Ravelo, 2013) operating as BP NGD function are considered. The proposed bridged-T circuit is presenting an advantage in terms of design simplicity and also the

Table 4 Specific attenuations of the tested BP NGD C-shunt inductorless bridged-T circuit

Designation	Parameters	Simulation	Calculation	Measurement
Attenuation at the NGD center frequency	$T(f_o)$	−6.67 dB	−6.66 dB	−5.82 dB
Attenuation at the NGD optimal frequency	$T(f_{opt})$	−6.53 dB	−6.32 dB	−5.73 dB
Attenuation at the lower cut-off frequency	$T(f_a)$	−3.25 dB	−2.59 dB	−2.97 dB
Attenuation at the upper cut-off frequency	$T(f_b)$	−6.11 dB	−6.18 dB	−1.50 dB

Figure 13 Comparisons of simulated, calculated and measured GDs displayed in (a) large- and (b) narrow-band plots

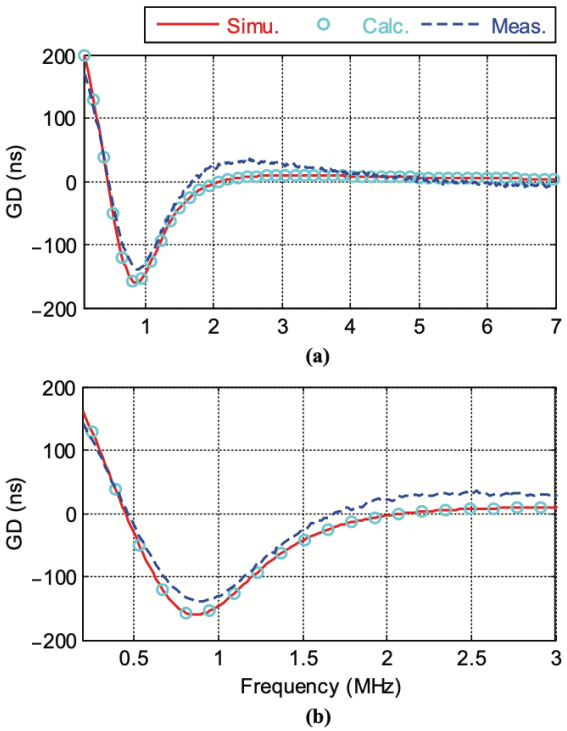

integrability because of the inductorless aspect. The drawback in terms of attenuation can be overcome with the more optimized circuit in the function of the expected BP NGD specifications.

5. Discussion on negative group delay circuit potential applications

Most of the electronic communication systems (Vemagiri *et al.*, 2007; Wan *et al.*, 2019a) are a victim of undesirable GD effects in the operation signal frequency band. Because of the possibility to design miniaturized inductorless bridged-T circuits, the investigated BP NGD topology can potentially be useful for the delay effect reduction especially in the area of electronic communication engineering. We can cite three potential applications in the following paragraphs.

5.1 Group delay reduction with bandpass negative group delay circuit

Figure 14(a) illustrates the configuration of the cascaded combination of an electronic system supposed victim of degradation as undesirable delay effect with a BP NGD circuit. To reduce GD $GD_{AB} > 0$ induced by the electronic communication system introduced by Figure 14(b), we can apply the NGD circuit to operate as a neutralizer function (Ravelo, 2013). To do this, we can insert a BP NGD circuit with GD $GD_{BC} < 0$. Then, the total GD GD_{AC} should be less significant than GD_{AB} with correction $GD_{AC} < GD_{AB}$.

5.2 Signal distortion correction by using bandpass negative group delay circuit

The BP NGD circuit can be originally used for the RF and microwave signal distortion correction (Ravelo *et al.*, 2020b). Figure 15 illustrates the waveform of the input ($Signal_A$), distorted ($Signal_B$) and corrected ($Signal_C$) signals. Because of the proposed NGD application technique, it can be expected that the corrected signal, $Signal_C$, should be well-correlated to the input one.

5.3 Resonance effect reduction by using bandpass negative group delay circuits

The BP NGD signal can also be very useful in the area of electromagnetic compatibility engineering of electronic circuits

Table 5 NGD specifications of the tested BP NGD circuit

Designation	Parameters	Simulation	Calculation	Measurement
NGD center frequency	f_o (MHz)	0.97	0.98	0.96
GD at the NGD center frequency	$\tau(f_o)$ (ns)	−151.60	−154.50	−134.60
NGD lower cut-off frequency	f_a (MHz)	0.44	0.14	0.46
NGD upper cut-off frequency	f_b (MHz)	2.12	2.21	1.73
NGD bandwidth	BW (MHz)	1.68	2.07	1.27
NGD optimal frequency	f_{opt} (MHz)	0.86	0.81	0.88
GD at the NGD optimal frequency	τ_{min} (ns)	−160.30	−157.20	−138.70

Table 4 Specific attenuations of the tested BP NGD C-shunt inductorless bridged-T circuit

Designation	Parameters	Simulation	Calculation	Measurement
Attenuation at the NGD center frequency	$T(f_o)$	−6.67 dB	−6.66 dB	−5.82 dB
Attenuation at the NGD optimal frequency	$T(f_{opt})$	−6.53 dB	−6.32 dB	−5.73 dB
Attenuation at the lower cut-off frequency	$T(f_a)$	−3.25 dB	−2.59 dB	−2.97 dB
Attenuation at the upper cut-off frequency	$T(f_b)$	−6.11 dB	−6.18 dB	−1.50 dB

Figure 13 Comparisons of simulated, calculated and measured GDs displayed in (a) large- and (b) narrow-band plots

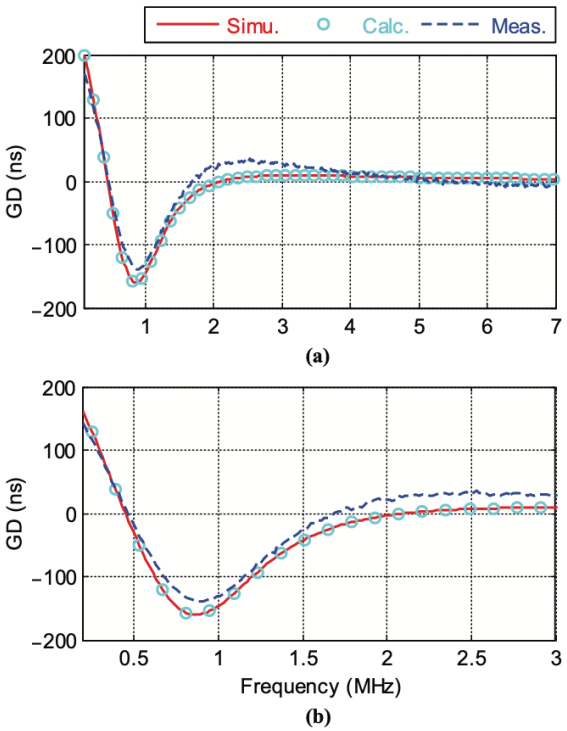

integrability because of the inductorless aspect. The drawback in terms of attenuation can be overcome with the more optimized circuit in the function of the expected BP NGD specifications.

5. Discussion on negative group delay circuit potential applications

Most of the electronic communication systems (Vemagiri *et al.*, 2007; Wan *et al.*, 2019a) are a victim of undesirable GD effects in the operation signal frequency band. Because of the possibility to design miniaturized inductorless bridged-T circuits, the investigated BP NGD topology can potentially be useful for the delay effect reduction especially in the area of electronic communication engineering. We can cite three potential applications in the following paragraphs.

5.1 Group delay reduction with bandpass negative group delay circuit

Figure 14(a) illustrates the configuration of the cascaded combination of an electronic system supposed victim of degradation as undesirable delay effect with a BP NGD circuit. To reduce GD $GD_{AB} > 0$ induced by the electronic communication system introduced by Figure 14(b), we can apply the NGD circuit to operate as a neutralizer function (Ravelo, 2013). To do this, we can insert a BP NGD circuit with GD $GD_{BC} < 0$. Then, the total GD GD_{AC} should be less significant than GD_{AB} with correction $GD_{AC} < GD_{AB}$.

5.2 Signal distortion correction by using bandpass negative group delay circuit

The BP NGD circuit can be originally used for the RF and microwave signal distortion correction (Ravelo *et al.*, 2020b). Figure 15 illustrates the waveform of the input ($Signal_A$), distorted ($Signal_B$) and corrected ($Signal_C$) signals. Because of the proposed NGD application technique, it can be expected that the corrected signal, $Signal_C$, should be well-correlated to the input one.

5.3 Resonance effect reduction by using bandpass negative group delay circuits

The BP NGD signal can also be very useful in the area of electromagnetic compatibility engineering of electronic circuits

Table 5 NGD specifications of the tested BP NGD circuit

Designation	Parameters	Simulation	Calculation	Measurement
NGD center frequency	f_o (MHz)	0.97	0.98	0.96
GD at the NGD center frequency	$\tau(f_o)$ (ns)	−151.60	−154.50	−134.60
NGD lower cut-off frequency	f_a (MHz)	0.44	0.14	0.46
NGD upper cut-off frequency	f_b (MHz)	2.12	2.21	1.73
NGD bandwidth	BW (MHz)	1.68	2.07	1.27
NGD optimal frequency	f_{opt} (MHz)	0.86	0.81	0.88
GD at the NGD optimal frequency	τ_{min} (ns)	−160.30	−157.20	−138.70

Table 4 Specific attenuations of the tested BP NGD C-shunt inductorless bridged-T circuit

Designation	Parameters	Simulation	Calculation	Measurement
Attenuation at the NGD center frequency	$T(f_o)$	−6.67 dB	−6.66 dB	−5.82 dB
Attenuation at the NGD optimal frequency	$T(f_{opt})$	−6.53 dB	−6.32 dB	−5.73 dB
Attenuation at the lower cut-off frequency	$T(f_a)$	−3.25 dB	−2.59 dB	−2.97 dB
Attenuation at the upper cut-off frequency	$T(f_b)$	−6.11 dB	−6.18 dB	−1.50 dB

Figure 13 Comparisons of simulated, calculated and measured GDs displayed in (a) large- and (b) narrow-band plots

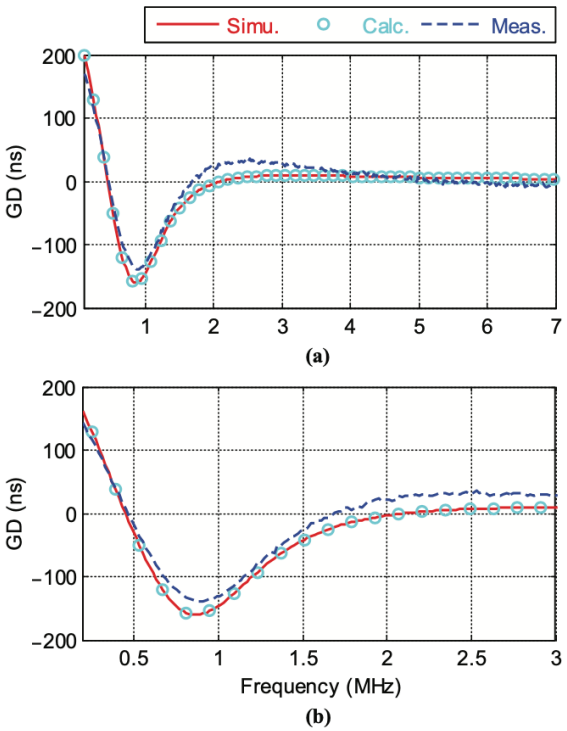

integrability because of the inductorless aspect. The drawback in terms of attenuation can be overcome with the more optimized circuit in the function of the expected BP NGD specifications.

5. Discussion on negative group delay circuit potential applications

Most of the electronic communication systems (Vemagiri *et al.*, 2007; Wan *et al.*, 2019a) are a victim of undesirable GD effects in the operation signal frequency band. Because of the possibility to design miniaturized inductorless bridged-T circuits, the investigated BP NGD topology can potentially be useful for the delay effect reduction especially in the area of electronic communication engineering. We can cite three potential applications in the following paragraphs.

5.1 Group delay reduction with bandpass negative group delay circuit

Figure 14(a) illustrates the configuration of the cascaded combination of an electronic system supposed victim of degradation as undesirable delay effect with a BP NGD circuit. To reduce GD $GD_{AB} > 0$ induced by the electronic communication system introduced by Figure 14(b), we can apply the NGD circuit to operate as a neutralizer function (Ravelo, 2013). To do this, we can insert a BP NGD circuit with GD $GD_{BC} < 0$. Then, the total GD GD_{AC} should be less significant than GD_{AB} with correction $GD_{AC} < GD_{AB}$.

5.2 Signal distortion correction by using bandpass negative group delay circuit

The BP NGD circuit can be originally used for the RF and microwave signal distortion correction (Ravelo *et al.*, 2020b). Figure 15 illustrates the waveform of the input ($Signal_A$), distorted ($Signal_B$) and corrected ($Signal_C$) signals. Because of the proposed NGD application technique, it can be expected that the corrected signal, $Signal_C$, should be well-correlated to the input one.

5.3 Resonance effect reduction by using bandpass negative group delay circuits

The BP NGD signal can also be very useful in the area of electromagnetic compatibility engineering of electronic circuits

Table 5 NGD specifications of the tested BP NGD circuit

Designation	Parameters	Simulation	Calculation	Measurement
NGD center frequency	f_o (MHz)	0.97	0.98	0.96
GD at the NGD center frequency	$\tau(f_o)$ (ns)	−151.60	−154.50	−134.60
NGD lower cut-off frequency	f_a (MHz)	0.44	0.14	0.46
NGD upper cut-off frequency	f_b (MHz)	2.12	2.21	1.73
NGD bandwidth	BW (MHz)	1.68	2.07	1.27
NGD optimal frequency	f_{opt} (MHz)	0.86	0.81	0.88
GD at the NGD optimal frequency	τ_{min} (ns)	−160.30	−157.20	−138.70

Transactions on Circuits and Systems II: Express Briefs, Vol. 68 No. 7, pp. 1-5.

Toumazou, C., Moschytz, G.S. and Gilbert, B. (2002), *Trade-Offs in Analog Circuit Design: The Designer's Companion*, Kluwer Academic Publishers.

Twin-T Notch Filter Design Tool (2020) "OKAWA electric design", http://sim.okawa-denshi.jp/en/TwinTCRkeisan.htm, (accessed Apr. 2020).

Vemagiri, J., Chamarti, A., Agarwal, M. and Varahramyan, K. (2007), "Transmission line Delay-Based radio frequency identification (RFID) tag", *Microwave and Optical Technology Letters*, Vol. 49 No. 8, pp. 1900-1904.

Wan, F., Wang, L., Ji, Q. and Ravelo, B. (2019a), "Canonical transfer function of band-pass NGD circuits", *IET Circuits, Devices & Systems*, Vol. 13 No. 2, pp. 125-130.

Wan, F., Wang, J., Ravelo, B., Ge, J. and Li, B. (2019b), "Time-domain experimentation of NGD active RC-Network cell", *IEEE Transactions on Circuits and Systems II: Express Briefs*, Vol. 66 No. 4, pp. 562-566.

Wang, Y.-R. and Lin, Y.-S. (2019), "Size-reduction of dual-wideband bandpass filters using Bridged-T coils", *IEEE Access*, Vol. 7 No. March, pp. 42836-42845.

Yao, B.Y., Zhou, Y.G., Cao, Q.S. and Chen, Y.C. (2009), "Compact UWB bandpass filter with improved upper-stopband performance", *IEEE Microw. Wireless Comp. Lett*, Vol. 19 No. 1, pp. 27-29.

Corresponding author

Sébastien Lallechere can be contacted at: sebastien.lallechere@uca.fr